

SIMRP: Self-Interference Mitigation Using RIS and Phase Shifter Network

Wei Zhang¹, Ding Chen¹, Bin Zhou¹, Yi Jiang², Zhiyong Bu¹

¹Shanghai Institute of Microsystem and Information Technology, Chinese Academy of Sciences, Shanghai, China

Email: wzhang@mail.sim.ac.cn, chending2001@163.com, {bin.zhou, zhiyong.bu}@mail.sim.ac.cn

²School of Information Science and Technology, Fudan University, Shanghai, China

Email: yijiang@fudan.edu.cn

Abstract—Strong self-interference due to the co-located transmitter is the bottleneck for implementing an in-band full-duplex (IBFD) system. If not adequately mitigated, the strong interference can saturate the receiver’s analog-digital converters (ADCs) and hence void the digital processing. This paper considers utilizing a reconfigurable intelligent surface (RIS), together with a receiving (Rx) phase shifter network (PSN), to mitigate the strong self-interference through jointly optimizing their phases. This method, named self-interference mitigation using RIS and PSN (SIMRP), can suppress self-interference to avoid ADC saturation effectively and therefore improve the sum rate performance of communication systems, as verified by the simulation studies.

Index Terms—in-band full-duplex, self-interference mitigation, reconfigurable intelligent surface, phase shifter network.

I. INTRODUCTION

Through transmitting (Tx) and receiving (Rx) signals in the same frequency band simultaneously, an in-band full-duplex (IBFD) system can achieve twice the capacity of its counterpart working in either a time division duplex (TDD) mode or a frequency division duplex (FDD) mode. In practice, however, the strong self-interference, caused by the co-located transmitter, can saturate the receiver’s analog-digital converters (ADCs), and hence void the subsequent digital signal processing of the co-located receiver [1]. Therefore, it is a prerequisite to mitigate the strong self-interference before the ADCs for implementing a real IBFD system.

In the past decades, numerous approaches have been proposed for self-interference mitigation (SIM). Initially, the papers [2] adopted symmetric placement of antennas to mitigate self-interference, but only for narrowband signals. Some researchers proposed to create a copy of self-interference and subtract it from the received signal before the ADCs, where the copy can be reconstructed from the digital domain [3] or the radio frequency (RF) domain [4]. However, due to hardware overheads, these analog SIM techniques do not apply to multi-input multi-output (MIMO) systems. Hence the paper [5] proposed to optimize the Tx beamforming matrix to null the effective channel of the strong self-interference for MIMO systems. Moreover, the emergence of reconfigurable intelligent surfaces (RISs) has opened up new possibilities for SIM.

For example, the paper [6] utilized RIS to mitigate the self-interference with a Rx antenna and a Tx antenna and built a prototype that can achieve the SIM amount of 85dB. The paper [7] proposed to optimize the Tx beamforming matrix and RIS coefficients for SIM of a RIS-assisted IBFD (RAIBFD) system, which has over 80% gain of sum rate compared with the traditional FDD system, but utilizing Tx beamforming matrix for SIM also reduces the downlink (DL) capacity [7, Fig. 6], which is undesirable as the transmission demand of DL data is much stronger than that of uplink in cellular networks.

Analog phase shifter network (PSN), deployed in between the Rx antennas and the ADCs, shows great compatibility with the MIMO systems, making it a perfect tool to mitigate the strong self-interference for future IBFD systems. In [8], the authors utilized RIS and PSN to enhance the spectral efficiency for full-duplex mmWave MIMO systems, but it did not consider the effect of finite bit resolution of ADC, and therein the SIM is not conducted before the ADCs.

This paper considers a RIS-assisted IBFD transceiver equipped with a PSN at Rx RF chains, and we propose to jointly optimize the phases of RIS and PSN to null the effective channel of the self-interference before the Rx ADCs, which is called self-interference mitigation using RIS and PSN (SIMRP). Compared with the RAIBFD system proposed in [7], the proposed SIMRP can release the downlink capacity potential and thus increase the sum rate of the IBFD system, as verified in the simulation results where the proposed SIMRP has a 33% gain of sum rate over the RAIBFD, 70% gain of sum rate over the conventional RIS-assisted FDD (RAFDD) system, and also reaches 95% of the sum rate of the ideal IBFD system equipped with ∞ -bit ADCs.

II. SIGNAL MODEL AND PROBLEM FORMULATION

A. Signal Model

We consider the self-interference mitigation (SIM) for an in-band full-duplex (IBFD) transceiver aided by a co-located M_{ris} -element RIS as shown in Fig. 1. The transceiver consists of M_t transmitting (Tx) antennas, M_r receiving (Rx) antennas, and N_{RF} Rx radio frequency (RF) chains. An analog phase shifter network (PSN), denoted as $\mathbf{F}_{RF} \in \mathcal{S}^{N_{RF} \times M_r}$ with $\mathcal{S} = \{e^{j\theta} | \theta \in \mathbb{R}\}$ and $N_{RF} \leq M_r$, is deployed in between the Rx antennas and the ADCs. Denote the channel from the Tx

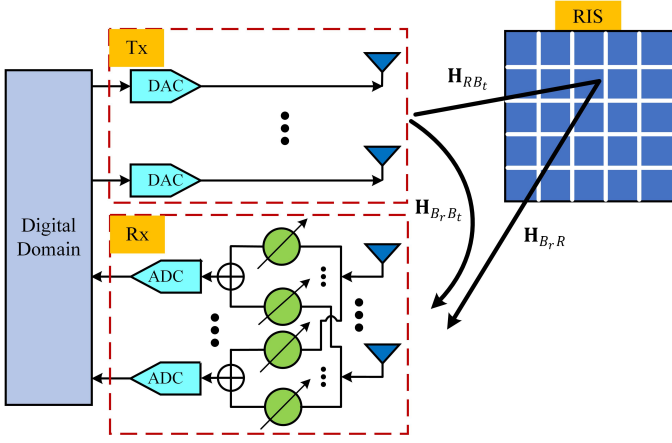


Fig. 1. The proposed IBFD transceiver structure.

antennas to the Rx antennas as $\mathbf{H}_{B_r B_t} \in \mathbb{C}^{M_r \times M_t}$, the channel from the Tx antennas to the RIS as $\mathbf{H}_{R B_t} \in \mathbb{C}^{M_{ris} \times M_t}$ and the channel from the RIS to the Rx antennas as $\mathbf{H}_{B_r R} \in \mathbb{C}^{M_r \times M_{ris}}$. Since the RIS channel estimation techniques have been widely investigated [9] [10], we assume the channel state information (CSI) to be perfectly known in the rest of this paper.

As the Tx antennas emit signal $\mathbf{s} \in \mathbb{C}^{M_t \times 1}$, the self-interference at the output of the PSN (but before the ADCs) can be denoted as

$$\xi = \mathbf{F}_{RF}(\mathbf{H}_{B_r R} \mathbf{D} \mathbf{H}_{R B_t} + \mathbf{H}_{B_r B_t}) \mathbf{s}, \quad (1)$$

where $\mathbf{D} = \text{diag}(e^{j\phi_1}, e^{j\phi_2}, \dots, e^{j\phi_{M_{ris}}})$ represents the adjustable phases of the RIS elements.

B. Problem Formulation

As the self-interference, along with the uplink signal, enters the Rx ADCs, the relations between the input signal-to-interference ratio (SIR) and the output signal-to-quantization-plus-noise ratio (SQNR) can be denoted as [11]

$$\text{SQNR}_{\text{dB}} \approx \text{SIR}_{\text{dB}} + 6.02 \text{ENOB} - 4.35, \quad (2)$$

where ENOB represents the effective number of bits of ADCs. According to (2), a self-interference of 30dBm may lead to quantization noise of $30 - 72 + 4.35 = -37.65\text{dBm}$ given that $\text{ENOB} = 12$, which shows that the self-interference mitigation (SIM) should be conducted before the Rx ADCs. To this end, we propose a SIM method named self-interference mitigation using RIS and PSN (SIMRP), which aims to jointly optimize the RIS coefficients \mathbf{D} and the PSN \mathbf{F}_{RF} to null the effective channel of the self-interference, i.e., to solve

$$\min_{\mathbf{D}, \mathbf{F}_{RF}} \|\mathbf{F}_{RF}(\mathbf{H}_{B_r R} \mathbf{D} \mathbf{H}_{R B_t} + \mathbf{H}_{B_r B_t})\|_F^2, \quad (3a)$$

$$\text{s.t. } \mathbf{D} = \text{diag}(e^{j\phi_1}, e^{j\phi_2}, \dots, e^{j\phi_{M_{ris}}}), \quad (3b)$$

$$\mathbf{F}_{RF} \mathbf{F}_{RF}^H = M_r \mathbf{I}, \quad (3c)$$

$$\mathbf{F}_{RF} \in \mathcal{S}^{N_{RF} \times M_r}, \quad (3d)$$

where (3c) ensures that N_{RF} dimensions of subspace are reserved for uplink signal transmission (cf. [5, (4)]). Given that (3) is non-convex and the optimal solution appears intractable, we propose an alternating optimization method to obtain its near-optimal solution.

III. ALGORITHM FOR OPTIMIZING THE COEFFICIENTS OF RIS AND PSN

In this section, we propose an alternating optimization method to solve (3), and obtain a near-optimal solution of \mathbf{D} and \mathbf{F}_{RF} .

A. The Optimization of \mathbf{D}

Fixing \mathbf{F}_{RF} , we have from (3) that

$$\begin{aligned} \min_{\mathbf{D}} \quad & \|\mathbf{A} \mathbf{D} \mathbf{H}_{R B_t} + \mathbf{B}\|_F^2, \\ \text{s.t.} \quad & \mathbf{D} = \text{diag}(e^{j\phi_1}, e^{j\phi_2}, \dots, e^{j\phi_{M_{ris}}}), \end{aligned} \quad (4)$$

where $\mathbf{A} = \mathbf{F}_{RF} \mathbf{H}_{B_r R} \in \mathbb{C}^{N_{RF} \times M_{ris}}$ and $\mathbf{B} = \mathbf{F}_{RF} \mathbf{H}_{B_r B_t} \in \mathbb{C}^{N_{RF} \times M_t}$. Using the formula $\text{vec}(\mathbf{XYZ}) = (\mathbf{Z}^T * \mathbf{X})\mathbf{y}$ where $\mathbf{Y} = \text{diag}(\mathbf{y})$ is a diagonal matrix with \mathbf{y} being its diagonal elements and $*$ represents Khatri-Rao product, we have the equivalent form of (4) as

$$\min_{\mathbf{d}} f(\mathbf{d}) \triangleq \|\mathbf{C} \mathbf{d} + \mathbf{b}\|_2^2, \quad (5a)$$

$$\text{s.t. } \mathbf{d} = [e^{j\phi_1}, e^{j\phi_2}, \dots, e^{j\phi_{M_{ris}}}]^T, \quad (5b)$$

where $\mathbf{C} = \mathbf{H}_{R B_t}^T * \mathbf{A} \in \mathbb{C}^{M_t N_{RF} \times M_{ris}}$, $\mathbf{b} = \text{vec}(\mathbf{B})$, and $\text{vec}(\mathbf{B})$ stands for the column vector obtained by stacking the columns of \mathbf{B} into a single column.

As the constant modulus of the variable \mathbf{d} defines a manifold

$$\mathcal{M}_{cc}^{M_{ris}} \triangleq \{\mathbf{d} \in \mathbb{C}^{M_{ris}} : |\mathbf{d}(1)| = \dots = |\mathbf{d}(M_{ris})| = 1\}, \quad (6)$$

we can solve (5) using the Riemannian conjugate gradient (RCG) algorithm, which can obtain a suboptimal solution as follows. The Riemannian gradient of $f(\mathbf{d})$ is defined as $\text{grad}(\mathbf{d}) \triangleq \nabla f(\mathbf{d}) - \text{Re}\{\nabla f(\mathbf{d}) \circ \mathbf{d}^*\} \circ \mathbf{d}$, where the Euclidean gradient $\nabla f(\mathbf{d})$ is

$$\nabla f(\mathbf{d}) = \mathbf{C}^H (\mathbf{C} \mathbf{d} + \mathbf{b}), \quad (7)$$

and \circ represents the Hadamard product. Starting from point \mathbf{d}_i in the i -th iteration with Riemannian gradient $\mathbf{g}_i = \text{grad}(\mathbf{d}_i)$, we can reach another point as

$$\mathbf{t}_i = \mathbf{d}_i + \alpha_i \mathbf{c}_i, \quad (8)$$

where α_i is the step size obtained using the Armijo-Goldstein condition and \mathbf{c}_i is the conjugate direction defined as

$$\mathbf{c}_i \triangleq \begin{cases} -\mathbf{g}_0, & i = 0, \\ -\mathbf{g}_i + \beta_i \mathbf{c}_{i-1}^+, & i \geq 1. \end{cases} \quad (9)$$

$\beta_i \triangleq \frac{\|\mathbf{g}_i\|_2^2}{\|\mathbf{g}_{i-1}^+\|_2^2}$, \mathbf{c}_{i-1}^+ and \mathbf{g}_{i-1}^+ are obtained as

$$\begin{aligned} \mathbf{c}_{i-1}^+ &= \mathbf{c}_{i-1} - \text{Re}\{\mathbf{c}_{i-1} \circ \mathbf{d}_i^*\} \circ \mathbf{d}_i, \quad i \geq 1, \\ \mathbf{g}_{i-1}^+ &= \mathbf{g}_{i-1} - \text{Re}\{\mathbf{g}_{i-1} \circ \mathbf{d}_i^*\} \circ \mathbf{d}_i, \quad i \geq 1. \end{aligned} \quad (10)$$

Then we map \mathbf{t}_i onto the manifold from (6), i.e., $\text{Retr}_{\mathcal{M}_{cc}^{M_{ris}}}(\mathbf{t}_i) \triangleq \left[\frac{\mathbf{t}_i(1)}{|\mathbf{t}_i(1)|}, \frac{\mathbf{t}_i(2)}{|\mathbf{t}_i(2)|}, \dots, \frac{\mathbf{t}_i(M_{ris})}{|\mathbf{t}_i(M_{ris})|} \right]^T$, and \mathbf{d}_i can be updated as $\mathbf{d}_{i+1} = \text{Retr}_{\mathcal{M}_{cc}^{M_{ris}}}(\mathbf{t}_i)$. Iterating i from 0 to ∞ until $f(\mathbf{d})$ improves less than ϵ_1 , e.g., $\epsilon_1 = 10^{-5}$, a near-optimal solution \mathbf{d} can be obtained over the Riemannian manifold.

B. The Optimization of \mathbf{F}_{RF}

Given that \mathbf{D} is obtained, we rewrite (3) as

$$\begin{aligned} \min_{\mathbf{F}_{\text{RF}}} \quad & \|\mathbf{F}_{\text{RF}} \mathbf{G}\|_{\text{F}}^2, \\ \text{s.t.} \quad & \mathbf{F}_{\text{RF}} \mathbf{F}_{\text{RF}}^H = M_r \mathbf{I}_{N_{\text{RF}}}, \end{aligned} \quad (11a)$$

$$\mathbf{F}_{\text{RF}} \in \mathcal{S}^{N_{\text{RF}} \times M_r}, \quad (11b)$$

where $\mathbf{G} = \mathbf{H}_{B_r R} \mathbf{D} \mathbf{H}_{R B_t} + \mathbf{H}_{B_r B_t} \in \mathbb{C}^{M_r \times M_t}$. Denoting $\mathbf{F}_{\text{RF}} \triangleq [\mathbf{f}_1, \mathbf{f}_2, \dots, \mathbf{f}_{N_{\text{RF}}}]^H$, we can divide (11) into N_{RF} subproblems, i.e.,

$$\begin{aligned} \min_{\mathbf{f}_1} \quad & \mathbf{f}_1^H \mathbf{G} \mathbf{G}^H \mathbf{f}_1, \\ \text{s.t.} \quad & \mathbf{f}_1 \in \mathcal{S}^{N_{\text{RF}} \times 1}, \end{aligned} \quad (12)$$

and

$$\begin{aligned} \min_{\mathbf{f}_m} \quad & \mathbf{f}_m^H \mathbf{G} \mathbf{G}^H \mathbf{f}_m, m = 2, \dots, N_{\text{RF}}, \\ \text{s.t.} \quad & \mathbf{f}_m^H \mathbf{F}_{m-1}^H \mathbf{F}_{m-1} \mathbf{f}_m = 0, \end{aligned} \quad (13a)$$

$$\mathbf{f}_m \in \mathcal{S}^{N_{\text{RF}} \times 1}, \quad (13b)$$

where $\mathbf{F}_{m-1} = [\mathbf{f}_1, \mathbf{f}_2, \dots, \mathbf{f}_{m-1}]^H \in \mathbb{C}^{(m-1) \times M_r}$. The solution to (12) can also be obtained using the RCG algorithm, while the constraint (13a) makes (13) intractable. Thus we propose an iterative sequential quadratic programming (SQP) method based on trust-region to solve (13), which is detailed as follows. Denoting $\Theta_m = [\theta_{m,1}, \theta_{m,2}, \dots, \theta_{m,M_r}]^T$ where $\theta_{m,n}$ represents the phase of the (m,n) -th element of \mathbf{F}_{RF} , we can define $g(\Theta_m) \triangleq \mathbf{f}_m^H \mathbf{G} \mathbf{G}^H \mathbf{f}_m$ and $h(\Theta_m) \triangleq \mathbf{f}_m^H \mathbf{F}_{m-1}^H \mathbf{F}_{m-1} \mathbf{f}_m$, and thus reformulate (13) into

$$\min_{\Theta_m} g(\Theta_m), \quad (14a)$$

$$\text{s.t.} \quad h(\Theta_m) = 0. \quad (14b)$$

Given the point $\Theta_{m,k}$ in the k -th iteration, the Lagrange function of (14) is $\mathcal{L}(\Theta_{m,k}, \lambda_{m,k}) = g(\Theta_{m,k}) + \lambda_{m,k} h(\Theta_{m,k})$ with $\lambda_{m,k}$ being the Lagrange multiplier. Letting $\nabla \mathcal{L}(\Theta_{m,k}, \lambda_{m,k}) = 0$, we have

$$\lambda_{m,k} = -\frac{\mathbf{h}_{m,k}^T \mathbf{g}_{m,k}}{\|\mathbf{h}_{m,k}\|_2^2}, \quad (15)$$

where $\mathbf{g}_{m,k}$ and $\mathbf{h}_{m,k}$ represent $\nabla g(\Theta_{m,k})$ and $\nabla h(\Theta_{m,k})$ and can be obtained as

$$\begin{aligned} \mathbf{g}_{m,k} &= -2\text{Im}((\mathbf{E} \mathbf{f}_{m,k}^*) \odot \mathbf{f}_{m,k}), \\ \mathbf{h}_{m,k} &= -2\text{Im}((\mathbf{J}_m \mathbf{f}_{m,k}^*) \odot \mathbf{f}_{m,k}), \end{aligned} \quad (16)$$

with $\mathbf{f}_{m,k} = e^{j\Theta_{m,k}}$, $\mathbf{E} = \mathbf{G}^* \mathbf{G}^T$, and $\mathbf{J}_m = \mathbf{F}_{m-1}^T \mathbf{F}_{m-1}$. We update $\Theta_{m,k}$ using $\Theta_{m,k+1} = \Theta_{m,k} + \Delta\Theta_{m,k}$ where $\Delta\Theta_{m,k}$

is the variation step, and thus can further approximate (14) at point $\Theta_{m,k}$ as

$$\min_{\Delta\Theta_{m,k}} \mathbf{g}_{m,k}^T \Delta\Theta_{m,k} + \frac{1}{2} \Delta\Theta_{m,k}^T \mathbf{Q}_{m,k} \Delta\Theta_{m,k}, \quad (17a)$$

$$\text{s.t.} \quad \mathbf{h}_{m,k}^T \Delta\Theta_{m,k} + h(\Theta_{m,k}) = 0, \quad (17b)$$

$$\|\Delta\Theta_{m,k}\|_2 \leq \Omega_k, \quad (17c)$$

where $\mathbf{Q}_{m,k} = \nabla^2 g(\Theta_{m,k}) + \lambda_{m,k} \nabla^2 h(\Theta_{m,k})$; (17c) defines a trust-region that ensures that (17a) is accurate, and $\Omega_k > 0$ is the trust-region radius. Letting $\mathbf{S}_{m,k} = \mathbf{f}_{m,k} \mathbf{f}_{m,k}^H$, we have

$$\nabla^2 g(\Theta_{m,k}) = -2\text{Re}[\text{diag}((\mathbf{E} \mathbf{f}_{m,k}^*) \odot \mathbf{f}_{m,k}) - \mathbf{E} \odot \mathbf{S}_{m,k}], \quad (18)$$

$$\nabla^2 h(\Theta_{m,k}) = -2\text{Re}[\text{diag}((\mathbf{J}_m \mathbf{f}_{m,k}^*) \odot \mathbf{f}_{m,k}) - \mathbf{J}_m \odot \mathbf{S}_{m,k}]. \quad (19)$$

Noticing that $\mathbf{Q}_{m,k}$ may not be a semi-positive definite matrix, we cannot treat (17) as a convex problem. We divide $\Delta\Theta_{m,k}$ into [12]

$$\Delta\Theta_{m,k} = \gamma \mathbf{h}_{m,k} + \mathbf{Z}_{m,k} \mathbf{x}, \quad (20)$$

where $\gamma \in \mathbb{R}$ and $\mathbf{Z}_{m,k} \in \mathbb{R}^{M_r \times (M_r - 1)}$ is a matrix whose columns form a basis of the orthogonal space of $\mathbf{h}_{m,k}$ with $\mathbf{Z}_{m,k}^T \mathbf{Z}_{m,k} = \mathbf{I}$. Hence we have $\mathbf{h}_{m,k}^T \mathbf{Z}_{m,k} \mathbf{x} = 0$, leading to

$$\|\Delta\Theta_{m,k}\|_2^2 = \gamma^2 \|\mathbf{h}_{m,k}\|_2^2 + \|\mathbf{x}\|_2^2. \quad (21)$$

First, we obtain γ that satisfies (17b) and (17c). Inserting (20) into (17b) yields that $\gamma \|\mathbf{h}_{m,k}\|_2^2 + h(\Theta_{m,k}) = 0$, and thus we need to solve

$$\min_{\gamma} \varphi(\gamma) \triangleq (\gamma \|\mathbf{h}_{m,k}\|_2^2 + h(\Theta_{m,k}))^2, \quad (22a)$$

$$\text{s.t.} \quad -\xi \Omega_k \leq \gamma \|\mathbf{h}_{m,k}\|_2 \leq \xi \Omega_k, \quad (22b)$$

where ξ is a real number and $0 < \xi < 1$. As $\varphi(\gamma)$ is a quadratic function about γ , the closed-form solution to (22) can be obtained as

$$\gamma_{\text{opt}} = \begin{cases} \frac{\xi \Omega_k}{\|\mathbf{h}_{m,k}\|_2}, & -\frac{h(\Theta_{m,k})}{\xi \|\mathbf{h}_{m,k}\|_2} \geq \Omega_k, \\ -\frac{h(\Theta_{m,k})}{\|\mathbf{h}_{m,k}\|_2^2}, & -\Omega_k < -\frac{h(\Theta_{m,k})}{\xi \|\mathbf{h}_{m,k}\|_2} < \Omega_k, \\ -\frac{\xi \Omega_k}{\|\mathbf{h}_{m,k}\|_2}, & \frac{h(\Theta_{m,k})}{\xi \|\mathbf{h}_{m,k}\|_2} \geq \Omega_k. \end{cases} \quad (23)$$

Second, we aim to minimize (17a) by optimizing \mathbf{x} . According to (20) and (21), we have

$$\Delta\Theta_{m,k} = \mathbf{Z}_{m,k} \mathbf{x} + \gamma_{\text{opt}} \mathbf{h}_{m,k}, \quad (24)$$

$$\|\Delta\Theta_{m,k}\|_2^2 = \|\mathbf{x}\|_2^2 + \gamma_{\text{opt}}^2 \|\mathbf{h}_{m,k}\|_2^2. \quad (25)$$

Then inserting (24) into (17a) and (25) into (17c) yields that

$$\min_{\mathbf{x}} (\mathbf{g}_{m,k} + \gamma_{\text{opt}} \mathbf{Q}_{m,k} \mathbf{h}_{m,k})^T \mathbf{Z}_{m,k} \mathbf{x} + \frac{1}{2} \mathbf{x}^T \bar{\mathbf{Q}}_{m,k} \mathbf{x}, \quad (26a)$$

$$\text{s.t.} \quad \|\mathbf{x}\|_2 \leq \sqrt{\Omega_k^2 - \gamma_{\text{opt}}^2 \|\mathbf{h}_{m,k}\|_2^2}, \quad (26b)$$

where $\bar{\mathbf{Q}}_{m,k} = \mathbf{Z}_{m,k}^T \mathbf{Q}_{m,k} \mathbf{Z}_{m,k}$. We can obtain the approximate solution to (26) using the truncated conjugate gradient (TCG) method [13], from which we can further have $\Delta\Theta_{m,k}$ and $\Theta_{m,k+1}$. Iterating m from 2 to N_{rf} and k from 1 to ∞ until (11) improves less than ϵ_2 , e.g., 10^{-5} , we can obtain a

Algorithm 1 The Iterative SQP Method to Solve (13)

Input: \mathbf{G} , Ω_1 , ξ , ϵ_2 and initial $\Theta_{1,1}, \dots, \Theta_{N_{\text{RF}},1}$;
Output: The matrix \mathbf{F}_{RF} ;

- 1: Solve (12) to obtain \mathbf{f}_1 with the power method;
- 2: **for** $m = 2 : N_{\text{RF}}$ **do**
- 3: Set $k = 1$;
- 4: Calculate $\mathbf{g}_{m,1}$ and $\mathbf{h}_{m,1}$ from (16);
- 5: Calculate $\lambda_{m,1}$ from (15), and then obtain $\mathbf{Q}_{m,1}$ from (19);
- 6: **while** The cost function (17a) improves less than ϵ_2 . **do**
- 7: Obtain α_{opt} from (23), and calculate $\bar{\mathbf{Q}}_{m,k}$;
- 8: Obtain \mathbf{x} from (26) using the TCG method;
- 9: Calculate $\Delta\Theta_{m,k}$ from (20) with α_{opt} and \mathbf{x} ;
- 10: **if** $g(\Theta_{m,k} + \Delta\Theta_{m,k}) > g(\Theta_{m,k})$ **then**
- 11: $\Omega_{k+1} = 0.5\Omega_k$;
- 12: **else**
- 13: $\Theta_{m,k+1} = \Theta_{m,k} + \Delta\Theta_{m,k}$;
- 14: $k = k + 1$;
- 15: Calculate $\mathbf{g}_{m,k}$, $\mathbf{h}_{m,k}$, $\lambda_{m,k}$, and $\mathbf{Q}_{m,k}$;
- 16: **end if**
- 17: **end while**
- 18: $\mathbf{f}_m = e^{j\Theta_m}$, $\mathbf{F}_{\text{RF}}(m, :) = \mathbf{f}_m^H$;
- 19: **end for**

near-optimal solution to (11).

We summarize this iterative algorithm in Algorithm 1, where we reduce the radius of the trust-region in line 11 to increase the approximation accuracy of (17) and guarantee the convergence of Algorithm 1; $\mathbf{F}_{\text{RF}}(m, :)$ in line 18 denotes the m -th row of \mathbf{F}_{RF} . We also summarize the proposed alternating optimization between \mathbf{F}_{RF} and \mathbf{D} in Algorithm 2, where $\epsilon_3 = 10^{-5}$ in line 1 and $\mathcal{Q}(\cdot)$ in line 7 can quantize the vector element-wise to the grids $\{0, \frac{2\pi}{2^b}, \frac{4\pi}{2^b}, \dots, \frac{(2^b-1)2\pi}{2^b}\}$ for b -bit RIS coefficients.

Algorithm 2 Alternating Optimization between \mathbf{F}_{RF} and \mathbf{D}

Input: $\mathbf{H}_{B_r B_t}$, $\mathbf{H}_{B_r R}$, $\mathbf{H}_{R B_t}$, and initial \mathbf{F}_{RF} and \mathbf{D} ;
Output: The matrix \mathbf{D} and analog PSN \mathbf{F}_{RF} ;

- 1: **while** the cost function in (3) decreases less than ϵ_3 **do**
- 2: Obtain \mathbf{G} and perform Algorithm 1 to obtain \mathbf{F}_{RF} ;
- 3: Fix \mathbf{F}_{RF} and obtain \mathbf{d} using the RCG algorithm from Section III-A;
- 4: **if** $b = \infty$ **then**
- 5: $\mathbf{D} = \text{diag}(\mathbf{d})$.
- 6: **else**
- 7: $\mathbf{d}_q = e^{j\mathcal{Q}(\angle \mathbf{d})}$.
- 8: **if** $\|\mathbf{C}\mathbf{d}_q + \mathbf{b}\|_2^2 < \|\mathbf{C}\mathbf{d} + \mathbf{b}\|_2^2$ **then**
- 9: $\mathbf{D} = \text{diag}(\mathbf{d}_q)$.
- 10: **end if**
- 11: **end if**
- 12: **end while**

C. Complexity Analysis

The complexity of the proposed RCG algorithm mainly lies in the iterative calculation of (5a) and (7), of which the complexity is $\mathcal{O}(M_t N_{\text{RF}} M_{\text{ris}})$. Denote I_r as the number of iterations of the RCG algorithm and denote I_a as the average number of Armijo-Goldstein condition searches. Then the complexity of the RCG algorithm can be denoted as $T_{\text{rcg}} = \mathcal{O}(I_r(1 + I_a)M_t N_{\text{RF}} M_{\text{ris}})$, which grows linearly with the number of RIS elements. For Algorithm 1 that obtains \mathbf{F}_{RF} , the computational complexity of one inner iteration mainly lies in (16), (19), $\bar{\mathbf{Q}}_{m,k}$, and the TCG method, of which the complexity can be approximated as $\mathcal{O}(M_r^3 + I_c M_r^2)$ with I_c being the iteration number of the TCG method. Given the number of outer loop and inner loop are $N_{\text{RF}} - 1$ and I_s , the complexity of Algorithm 1 is $T_1 = \mathcal{O}((N_{\text{RF}} - 1)I_s(M_r^3 + I_c M_r^2))$. Hence the computational complexity of the Algorithm 2 is $T_{\text{tot}} = I_d(T_{\text{rcg}} + T_1)$, where I_d is the iteration number of Algorithm 2.

IV. SIMULATION RESULTS

For the following simulations, the RIS is placed behind the antenna plane as illustrated in Fig. 2, where both the Tx and Rx antennas are arranged into 8×1 uniform linear array (ULA), i.e., $M_r = M_t = 8$. The number of Rx RF chains is $N_{\text{RF}} = 3$. For both the antenna arrays and the RIS, the inter-element spacing is $\frac{\lambda}{2}$, where λ is the wavelength. Denote the distance between antennas and the RIS as d_{RA} , and the distance between the center of the transmit and receive antenna arrays as $d_{B_r B_t}$. We set $d_{B_r B_t} = 3\lambda$ and $d_{RA} = \frac{\lambda}{2}$ [7]. For wave number $k_\lambda = \frac{2\pi}{\lambda}$, the LOS near-field channel between two adjacent points $A(x_1, y_1, z_1)$ and $B(x_2, y_2, z_2)$ in Fig. 2 is simulated as [14]

$$h_{AB} = \sqrt{\beta_{AB}} e^{-jk_\lambda d_{AB}}, \quad (27)$$

where $\beta_{AB} = \frac{G_l}{4} \left(\frac{1}{(k_\lambda d_{AB})^2} - \frac{1}{(k_\lambda d_{AB})^4} + \frac{1}{(k_\lambda d_{AB})^6} \right)$, $G_l = 1$ given omnidirectional antenna, and

$$d_{AB} = \sqrt{(x_1 - x_2)^2 + (y_1 - y_2)^2 + (z_1 - z_2)^2}.$$

Hence the entries of $\mathbf{H}_{B_r R}$, $\mathbf{H}_{B_r B_t}$, and $\mathbf{H}_{R B_t}$ are so generated from (27). For all the following simulations, it is assumed that $\lambda = 0.125\text{m}$.

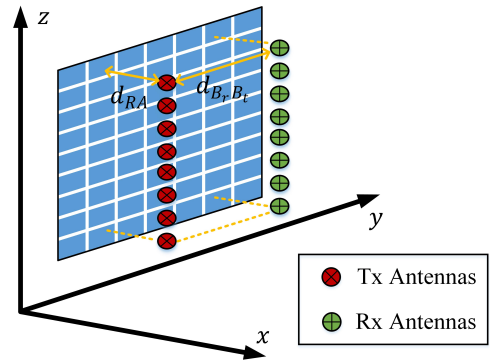


Fig. 2. The placement of the RIS and the antennas.

Consider that the IBFD transceiver shown in Fig. 2 serves as a macro BS and communicates with three uplink (UL) users and three downlink (DL) users simultaneously. Both the UL and the DL users are of single-antenna and are uniformly distributed [100m, 140m] away from the BS [15]; the channels from users to the BS, from users to the RIS are from Saleh-Valenzuela model with free space path loss; the Tx power of the BS is 30dBm, which is allocated with the well-known water-filling method and the zero-forcing precoding; the Tx power of UL users is 10dBm and the thermal noise of the BS and the DL users are -96dBm [16]. For Algorithm 1, we set $\xi = 0.6, \Omega_1 = 0.5$.

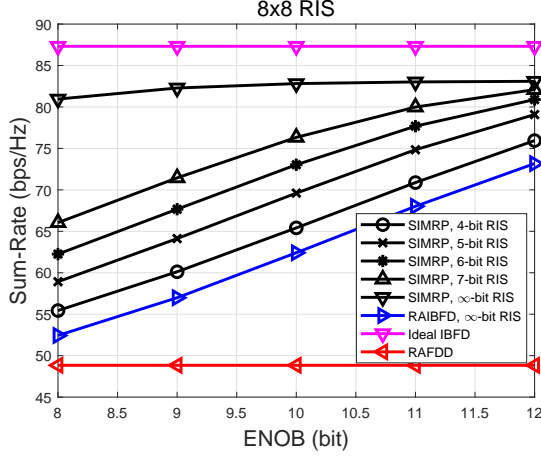


Fig. 3. The sum rate vs. the effective number of bits.

Given a 8×8 RIS, Fig. 3 compares the sum rate performance of the SIMRP with that of the RAIBFD, ideal IBFD proposed in [7] and RIS-assisted FDD (RAFDD) system, where the ideal IBFD system equipped with ∞ -bit ADCs and the RAFDD system provides an upper bound and a lower bound for the sum rate performance of the proposed SIMRP. Given ∞ -bit RIS, the sum rate of the proposed SIMRP system reaches 95% of that of the ideal IBFD as ADC's effective number of bits (ENOB) varies from 8 to 12, and outperforms the RAIBFD by around 33% at ENOB = 10. Even when using RIS of finite bit resolutions, i.e., $b = 4, 5, 6, 7$, the SIMRP still has a gain of sum rate over the RAIBFD with ∞ -bit RIS and the RAFDD system, but the RISs of lower bit resolution lead to larger performance degradation compared with the SIMRP with ∞ -bit RIS, especially when 8-bit and 9-bit ADC are deployed. As ∞ -bit PSN is considered in Fig. 3, we can utilize PSN of high resolutions to approach its performance, i.e., 8-bit PSN.

The second simulation studies the sum rate performance of the proposed SIMRP given imperfect channel state information (CSI), where the cascaded channels $\hat{\mathbf{H}}_{B_r R}$ and $\hat{\mathbf{H}}_{R B_t}$ are denoted as

$$\begin{aligned}\hat{\mathbf{H}}_{B_r R} &= \mathbf{H}_{B_r R} + \Delta \mathbf{H}_{B_r R} \in \mathbb{C}^{M_r \times M_{ris}}, \\ \hat{\mathbf{H}}_{R B_t} &= \mathbf{H}_{R B_t} + \Delta \mathbf{H}_{R B_t} \in \mathbb{C}^{M_{ris} \times M_t},\end{aligned}\quad (28)$$

with the entries of $\Delta \mathbf{H}_{B_r R}$ and $\Delta \mathbf{H}_{R B_t}$ following

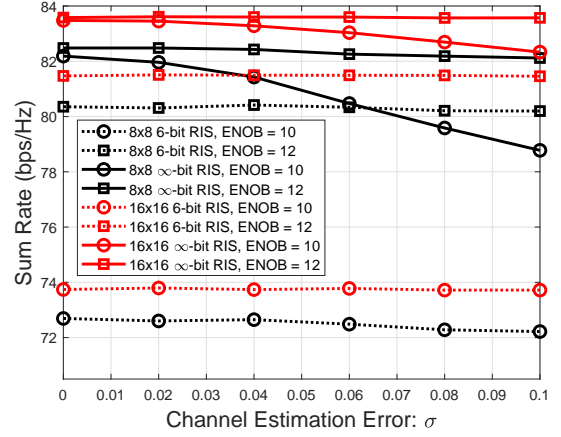


Fig. 4. The sum rate vs. channel estimation error.

$\mathcal{CN}(0, \frac{\|\mathbf{H}_{B_r R}\|_F^2}{M_r^2 M_{ris}^2} \sigma^2)$ and $\mathcal{CN}(0, \frac{\|\mathbf{H}_{R B_t}\|_F^2}{M_{ris}^2 M_t^2} \sigma^2)$. Fig. 4 shows the sum rate performance of the SIMRP under different RIS sizes (8×8 and 16×16) and different RIS resolutions (6-bit and ∞ -bit) given that ENOB = 10, 12, which shows that the SIMRP with RIS of larger size and ADC of reasonably high bit resolutions are robust to the channel estimation error.

V. CONCLUSION

In this paper, we propose a novel method, called self-interference mitigation using RIS and phase shifter network (SIMRP), where a co-located RIS and an analog phase shifter network (PSN) are utilized to mitigate the self-interference before the ADCs. We proposed to minimize the power of self-interference by jointly optimizing the phases of the RIS and the PSN. The simulation results show the proposed SIMRP method can effectively mitigate self-interference and outperform the state-of-the-art method.

REFERENCES

- [1] A. Sabharwal, P. Schniter, D. Guo, D. W. Bliss, S. Rangarajan, and R. Wichman, "In-band full-duplex wireless: Challenges and opportunities," *IEEE J. Sel. Areas Commun.*, vol. 32, no. 9, pp. 1637–1652, 2014.
- [2] J. I. Choi, M. Jain, K. Srinivasan, P. Levis, and S. Katti, "Achieving single channel, full duplex wireless communication," in *Proceedings of the Sixteenth Annual International Conference on Mobile Computing and Networking*, 2010, pp. 1–12.
- [3] T. Fukui, K. Komatsu, Y. Miyaji, and H. Uehara, "Analog self-interference cancellation using auxiliary transmitter considering IQ imbalance and amplifier nonlinearity," *IEEE Trans. Wireless Commun.*, vol. 19, no. 11, pp. 7439–7452, 2020.
- [4] C. W. Morgenstern, Y. Rong, A. Herschfeld, A. C. Molnar, A. B. Apsel, D. G. Landon, and D. W. Bliss, "Analog-domain self-interference cancellation for practical multi-tap full-duplex system: Theory, modeling, and algorithm," *IEEE J. Sel. Areas Commun.*, vol. 41, no. 9, pp. 2796–2807, 2023.
- [5] E. Everett, C. Shepard, L. Zhong, and A. Sabharwal, "SoftNull: Many-antenna full-duplex wireless via digital beamforming," *IEEE Trans. Wireless Commun.*, vol. 15, no. 12, p. 8077 – 8092, December 2016.
- [6] S. Tewes, M. Heinrichs, P. Staat, R. Kronberger, and A. Sezgin, "Full-duplex meets reconfigurable surfaces: RIS-assisted SIC for full-duplex radios," in *ICC 2022 - IEEE International Conference on Communications*, 2022, pp. 1106–1111.

- [7] W. Zhang, Z. Wen, C. Du, Y. Jiang, and B. Zhou, "RIS-assisted self-interference mitigation for in-band full-duplex transceivers," *IEEE Trans. Commun.*, vol. 71, no. 9, pp. 5444–5454, 2023.
- [8] S. Yang, W. Lyu, Y. Xanthos, Z. Zhang, C. Assi, and C. Yuen, "Reconfigurable intelligent surface-aided full-duplex mmwave MIMO: Channel estimation, passive and hybrid beamforming," *IEEE Trans. Wireless Commun.*, vol. 23, no. 4, pp. 2575–2590, 2024.
- [9] H. Liu, X. Yuan, and Y.-J. A. Zhang, "Matrix-calibration-based cascaded channel estimation for reconfigurable intelligent surface assisted multiuser MIMO," *IEEE J. Sel. Areas Commun.*, vol. 38, no. 11, pp. 2621–2636, 2020.
- [10] J. Tang, X. Du, Z. Chen, X. Zhang, D. K. C. So, K.-K. Wong, and J. A. Chambers, "Joint sparsity and low-rank minimization for reconfigurable intelligent surface-assisted channel estimation," *IEEE Trans. Commun.*, vol. 72, no. 3, pp. 1688–1700, 2024.
- [11] W. Zhang, Y. Jiang, B. Zhou, and D. Hu, "Hybrid interference mitigation using analog prewhitening," *IEEE Trans. Wireless Commun.*, vol. 20, no. 10, pp. 6595–6605, 2021.
- [12] N. I. M. Gould and S. Leyffer, *An Introduction to Algorithms for Nonlinear Optimization*. Berlin, Heidelberg: Springer Berlin Heidelberg, 2003, pp. 109–197. [Online]. Available: https://doi.org/10.1007/978-3-642-55692-0_4
- [13] T. Steihaug, "The conjugate gradient method and trust regions in large scale optimization," *SIAM Journal on Numerical Analysis*, vol. 20, no. 3, pp. 626–637, 1983.
- [14] H. Schantz, "Near field propagation law & a novel fundamental limit to antenna gain versus size," in *2005 IEEE Antennas and Propagation Society International Symposium*, vol. 3A, 2005, pp. 237–240.
- [15] Z. Peng, Z. Zhang, C. Pan, L. Li, and A. L. Swindlehurst, "Multiuser full-duplex two-way communications via intelligent reflecting surface," *IEEE Transactions on Signal Processing*, vol. 69, pp. 837–851, 2021.
- [16] E. Björnson and L. Sanguinetti, "Making cell-free massive MIMO competitive with MMSE processing and centralized implementation," *IEEE Trans. Wireless Commun.*, vol. 19, no. 1, pp. 77–90, 2020.